이학석사 학위논문

자폐 스펙트럼 장애환자 유도만능 줄기세포 유래 뉴런에서 세포학적 병인 및 기능연구

Study on cellular pathology and functions in induced pluripotent stem cell (iPSC)-derived neurons from an autism spectrum disorder (ASD) patient

2017년 2월

서울대학교 대학원

생명과학부

양 정 은

Study on cellular pathology and functions in induced pluripotent stem cell (iPSC)-derived neurons from an autism spectrum disorder (ASD) patient

Advisor. Professor Bong-Kiun Kaang

A dissertation submitted to the Graduate Faculty of Seoul National University in partial fulfillment of the requirement for the Degree of Master of Science

Jung-eun Yang

Graduate School of Natural Sciences

Seoul National University

Biological Sciences Major

Table of Contents

Page

List of Figures

Page

Abstract

Study on cellular pathology and functions in induced pluripotent stem cell (iPSC)-derived neurons from an autism spectrum disorder (ASD) patient

Jung-eun Yang

Department of Biological Sciences

The Graduate School

Seoul National University

Autism spectrum disorder (ASD) is a neurodevelopmental disorder which is characterized by difficulties in social communication, social interaction, repetitive and restricted behaviors. Most research on ASD until now has been based on mouse genetic models. However, due to the heterogeneity of ASD and the inadequacy of the mouse

model system, there were many cases that drugs verified in mouse model fail in clinical stage. In addition, ASD pathology was largely unknown. Recent technical advances in induced pluripotent stem cell (iPSC) fields enabled us to perform research on human cellular model system. In this study, we generated human neurons from ASD patient-derived iPSCs and investigated cellular phenotypes compared to human neurons from healthy people-derived iPSCs. Surprisingly, we found that NMDA currents were significantly reduced in ASD neurons by performing whole-cell patch clamp recording. In addition, the mRNA expressions of NMDAR subunits and CaMKII which is NMDAR downstream signaling molecule were significantly decreased in ASD neurons. Our finding suggests a possibility that ASD neurons are disrupted in NMDAR related signaling.

Keyword: Autism spectrum disorder, induced pluripotent stem cells (iPSCs), iPSC-derived neurons, cellular pathology, NMDA currents, NMDAR subunits, CaMKII.

Student Number: 2014-21279

Introduction

Autism spectrum disorder (ASD) is one of the neurodevelopmental disorders which is characterized by difficulties of social communication and social interaction and by repetitive behaviors. The recent prevalence of ASD was estimated to 14.6 per 1000 children aged 8 years in the United States and 2~3 per 100 school-age children in South Korea (Christensen et al., 2016; Kim et al., 2011). A lot of findings suggest genetic, environmental factors, and gene-environment interaction contribute to ASD (Croen et al., 2011; Fakhoury, 2015; Klauck, 2006; Lyall et al., 2014; Zhu et al., 2014). However, the exact causes of ASD are still unknown.

Recently, the technical development of genome-sequencing revealed *de novo* mutations and copy number variations of ASD (Abrahams and Geschwind, 2008). Several genetic mutations were demonstrated as ASD-risk factors using mouse genetic models (Bey and Jiang, 2014). Mouse models were used to study human diseases because mice share 95% of genes with humans and are easy to manipulate genomes. However, mouse phenotypes are different according as the targeted region on a same gene. Therefore, there are many cases that drugs verified in mouse model fail in clinical stage during new drug development.

One of the methods overcoming the limits of mouse disease model is using patient-derived induced pluripotent stem cells (iPSCs). Cell reprogramming technology have made possible neuroscientists to investigate previously inaccessible human neurons (Takahashi et al., 2007; Takahashi and Yamanaka, 2006; Yu et al., 2007). Research on human neurological disorders has increased explosively after advances in cell reprogramming technology. Before the advent of this technology, human-derived neurons had been obtained only after death in most neurological disorders except epilepsy. In other words, human cellular pathology could be investigated after patients' death. However, this technology enabled to study cellular pathology while patients are alive and try the patients-specific treatments. Based on these studies, many researchers have been culturing the neuropsychiatric patients-derived neurons in a dish. They have not only revealed causes of the disorders including schizophrenia, bipolar disorder, and various syndromes but also found drugs rescuing cellular deficits through drug screening (Mertens et al., 2015; Shcheglovitov et al., 2013; Wen et al., 2014).

DSM-5 (Diagnostic and Statistical Manual of Mental Disorders, 5th edition) recategorized ASD including autism, Asperger, and PDD-NOS (Pervasive Developmental Disorder - Not Otherwise Specified). As the name 'spectrum' suggests, ASD shows a broad range of symptoms based on social communication impairments and restricted, repetitive patterns of behavior. Cellular

pathology is also expected to show differences between patients with severity of symptoms.

In this study, we induced human neurons from an ASD patient-derived iPSCs and investigated cellular properties compared to human neurons from healthy people-derived iPSCs. Specifically, we performed patch clamp recording to investigate electrophysiological properties of neurons and qRT-PCR to confirm expression levels of specific genes.

Materials & Methods

1. Cell culture

ASD iPSC#1 (KH_A_025-1-1), ASD iPSC#2 (KH_A_025-1-2), Urinary iPSC, Foreskin iPSC were obtained from Hannam University. iPS cells (passage < 60) were cultured on irradiated MEFs (CF-1, ATCC) in human ES cell media consisting DMEM/F12 (Invitrogen), 20% Knockout Serum replacement (Invitrogen), 2 mM Glutamax (Invitrogen), 100 μM MEM NEAA(Invitrogen), 100 U/mL Penicillin/Steptomycin (HyClone), 385 nM β-mercaptoethanol (Invitrogen), and 5 ng/mL human basic FGF (PeproTech). Media were changed daily and iPS cell lines were passaged mechanically.

Mouse astrocytes were cultured from the cortex of postnatal P3 wild-type B6 mice. Briefly, mouse cortex homogenates were digested with 0.25% Trypsin, resuspended in HBSS (Invitrogen) containing 0.05% DNaseI, and plated onto T75 flasks in DMEM with 15% FBS. Media were changed every 2-3 days and glial cells were replated 3 times to remove non-astrocytes.

2. Virus generation

Lentiviral constructs, FUW-TetO-Ngn2-P2A-EGFP-T2A-Puromycin and FUW-rtTA, were kindly provided by Dr. Südhof (Stanford University, USA). Lentivirus were generated in HEK293T cells by cotransfection with two helper plasmids (psPAX2, pMD2.G) (13.3 ㎍ lentiviral vector DNA, 10 ㎍ psPAX2, and 3.3 ㎍ pMD2.G per 100 mm culture dish) using calcium phosphate. The media containing lentiviruses were harvested 48 hr and 72 hr after transfection, filtered with 0.45 ㎛ syringe filter, and centrifugated at 20,000 x g for 2 hr. The pellets were resuspended in DMEM/F12, aliquoted, and frozen in -80 ℃ deep freezer. Lentivirus titer was assessed by EGFP expression and used with > 80% infection efficiency.

3. Generation of induced neurons from human iPSCs

The protocol was illustrated in Fig.1A and based on the previously reported Ngn2 method (Zhang et al., 2013). Specifically, iPS-cell cultures were detached using accutase (Innovative Cell Tech) for 10 min and pre-plated on gelatin for 1 hr at 37 ℃ to remove MEFs (Gaspard et al., 2009). The supernatant iPS cells were collected carefully and plated on matrigel (BD, 1:20)-coated 6 well plate in

mTeSR1 media (Stem Cell Technologies) containing 10 μM Y-27632 (Tocris). On day -1, lentivirus was added in fresh mTeSR1 media. On day 0, the culture media were replaced with N2/DMEM/F12/NEAA (Invitrogen) containing 10 μg/L human BDNF (PeproTech), 10 μg/L human NT-3 (PeproTech), 0.2 ㎎/L laminin (Invitrogen), and 2 g/L doxycycline (Sigma) to induce TetO gene expression. On day 1, 1 ㎎/L puromycin was added to select virus-infected cells for 24 hr. On day 2, the culture media were replaced with astrocyte-conditioned media containing human BDNF, NT3, doxycycline and half of the media was replaced every 2 days until day 6. Astrocyte-conditioned media are Neurobasal/B27/Glutamax (Invitrogen) media incubated on the mouse astrocyte culture for 24 hr. On day 4, mouse astrocytes (10,000 cells / well) were plated on 24 well matrigel-coated coverslips. On day 7, iN cells were harvested and dissociated with Neubasal/B27/Glutamax media containing human BDNF, NT3, Doxycycline, and 1 μM Ara-C to inhibit astrocyte proliferation. iN cells (50,000 cells / well) were co-cultured onto astrocytes. After co-culture with astrocytes, Half of the media in each well was exchanged every 2-3 days and 2.5% FBS was added to support astrocyte viability. Most experiments were performed on 2 weeks after co-culture. Only measuring NMDA currents was performed on 6 weeks after co-culture.

4. Immunocytochemistry

Immunocytochemistry were performed as described (Yu et al., 2016). Briefly, iN cells were fixed in 4% paraformaldehyde/4% sucrose in PBS for 20 min at 4℃. These neurons were permeabilized with 0.3% Triton X-100, 0.1% BSA in PBS and then blocked with 0.08% Triton X-100, 2% BSA in PBS. Anti-MAP2 (1:500, Millipore, AB5622), anti-CaMKII (1:500, abcam, ab52476) were applied overnight at 4 ℃ and washed three times. Alexa fluor 594 (1:500, Invitrogen, A11012) was applied at room temperature for 2 hr and washed three time. Neurons were mounted on Vectashield with DAPI (VectorLab) and imaged using confocal microscope (LSM-700, Zeiss) and fluorescence microscope (IX51, Olympus). Data were analyzed using ImageJ.

5. Electrophysiology

Whole-cell patch-clamp recordings were basically performed as described (Shcheglovitov et al., 2013; Yu et al., 2016; Zhang et al., 2013). All recordings were performed at room temperature (23-25 ℃). Neurons were visualized with 40x on an Olympus microscope (BX51WI) and recorded using a Multiclamp 700B amplifier and pClamp 10.2 software (Molecular Devices). Data were

digitized at 10 kHz with a 2 kHz lowpass filter using Digidata 1440 16-bit A/D converter (Axon instruments). The recording pipettes (3-5 MΩ) were pulled with P-1000 (Sutter instrument) with three step protocol. Internal solution for the basic electrical properties contained 145 mM K-Gluconate, 5 mM NaCl, 0.2 mM EGTA, 10 mM HEPES, 2 mM MgATP, 0.1 mM Na3GTP, and 1 mM MgCl2 (pH 7.2 with KOH, 270-280 mOsm). Internal solution for measuring miniature excitatory postsynaptic currents (mEPSCs) and NMDA currents contained 120 mM Cs-Gluconate, 5 mM NaCl, 20 mM HEPES, 0.6 mM EGTA, 4 mM MgATP, 0.3 mM Na3GTP, and 5 mM TEA (pH 7.2 with CsOH, 270-280 mOsm). The bath solution in all experiments contained 140 mM NaCl, 5 mM KCl, 2 mM CaCl2, 2 mM MgCl2, 10 mM HEPES, and 10 mM Glucose (pH 7.4 with NaOH). For all experiments, 10 μM picrotoxin (Tocris) was added to the bath solution to block GABAA receptor mediated currents. For measuring mEPSCs, 1 μM tetrodotoxin (Alomone Labs) were more added to the bath solution to block evoked synaptic responses. For measuring NMDA currents, 10 μM picrotoxin and 10 μM CNQX (Tocris) to block AMPA/kainate receptor responses were more added to the bath solution. NMDA currents were induced by a focal transient application of 100 μM NMDA and 10 μM Glycine. An injection pipette was connected to a pico-injector (PLI-100, Medical Systems Corp.). Resistances were monitored and recording data were not used if it changed significantly (> 25%). Cells that required more than 200 pA of hold currents to maintain -70 mV

were excluded from the dataset. Data were analyzed using Clampfit 10.6 (Molecular Devices).

6. qPCR

Total RNA was isolated using RNeasy Mini Kit (Qiagen) according to the manufacturer' s instructions. cDNA was synthesized with the SuperScript III and random hexamers (Invitrogen). Real-time PCR was performed using SYBR premix ExTaqII (RR820A, Takara) in the 7300 Real-Time PCR System (Applied Biosystems). The primer sequences were as follows: GRIN1 (forward: ACC CCA AGA TCG TCA ACA TTG, reverse: GGC TAA CTA GGA TGG CGT AGA), GRIN2A (forward: TGG CCT CAC CGG GTA TGA TT, reverse: CAA TGC CGT CCC TCA CTC TC), GRIN2B (forward: GTC CCT GGA CGA TGG AGA TTC, reverse: CAG TCA GCC CTA CTG AGT TGG), CaMKIIa (forward: CAG TTC CAG CGTTCA GTT AAT G, reverse: TTC GTG TAG GAC TCA AAA TCT CC), and GAPDH (forward: GGA GCG AGA TCC CTC CAA AAT, reverse: GGC TGT TGT CAT ACT TCT CAT GG).

7. Statistics

All experimental data were analyzed using Graphpad Prism 5 software. Statistical comparisons were made using t-test and two-way ANOVA. Further comparison was performed by the post hoc Bonferroni test. p-values were as indicated. All data were presented as mean ± SEM.

Results

Generation of ASD patient-derived neurons

To investigate neuronal phenotypes of ASD in the human system, we used two iPS cell lines from an ASD patient that shows self-injury and repetitive behaviors and two iPS cell lines from two healthy people as controls. All clinically validated somatic cells were provided from Kyungpook University Hospital. All iPS cell lines were generated by using a standard reprogramming technique (Okita et al., 2011) in Dr. Jin-A Lee' s Lab of Hannam university. We differentiated normal and ASD iPSCs into neurons using a modified Ngn2 single-step induction method (Gaspard et al., 2009; Zhang et al., 2013) (Fig. 1A).

Specifically, on day -2, stem cells were plated. On day -1, TetO-Ngn2-P2A-EGFP-T2A-Puromycine lentivirus and rtTA lentivirus were treated to overexpress Ngn2. On day 0, doxycycline was added to induce gene expression. On day 1, virus-infected cells were selected by puromycin treatment. On day 2, media were replaced with astrocyte-conditioned media (ACM). Half of the culture media was changed with ACM every 2 days until day 6. On day 4, astrocytes were prepared on other plates. On day 7, neurons

were harvested and plated on the astrocyte culture. Half of media was changed every 2-3 days until experiments. Functional analyses including electrophysiological experiments, qPCR, and immunostaining were performed over 2 weeks after astrocyte co-culture (Fig. 1B). The main difference between the original and modified method is astrocytes co-culture. In the original method, astrocytes were added to each well culturing neuron. However, in the modified method, we counted the number of neurons and added the same number of neurons to each well culturing astrocyte to make up the same cell density on each well. Cell viability was different depending on iPS cell lines.

To confirm differentiated neurons, we stained both neurons derived ASD iPSC #1 and #2 for neuronal marker MAP2. GFP identified cells with viral transduction. Almost 100% of GFP positive cells showed MAP2 positive (Fig. 1C, D).

Intrinsic electrical properties and miniature excitatory postsynaptic currents were not altered in human ASD neurons.

To quantify the degree of neuronal maturation, we compared electrophysiological parameters between ASD and normal neurons on 2 weeks after co-culture by performing whole-cell patch-

clamp recording as described before (Chanda et al., 2014). If a neuron become mature, neuronal surface and ion channels are increased. Increased ion channels shift the resting membrane potential (RMP) toward −65 mV known as the mature neuronal RMP. Also, elevation of open ion channels decreases input resistance. The membrane capacitance is positive correlation with membrane surface (Hodgkin and Katz, 1949; Lamas et al., 2002; Pre et al., 2014). However, RMP, capacitance, and input resistance were not significantly changed in ASD neurons (Fig. 2). Also, voltage−gated sodium and potassium currents were similar between ASD and normal neurons (Fig. 3). In addition, action potential(AP) become faster and narrower when a neurons becomes mature (Maroof et al., 2013; Telias et al., 2014). However, ASD neurons did not show significantly differences with normal neurons in AP firing properties including AP number, threshold, amplitude, and half−width (Fig. 4). Thus, the maturation state of ASD neurons was similar with that of normal neurons at 2 weeks after co−culture.

To compare synaptic competence, we measured miniature excitatory postsynaptic currents (mEPSCs) in ASD and normal neurons. The amplitude and frequency of mEPSCs did not show significant differences (Fig. 5). Overall, these results suggest that normal and ASD neurons show similar maturation states not only intrinsically, but also synaptically.

NMDA currents and NMDAR mRNA expression levels were impaired in human ASD neurons.

Because behavioral symptoms of the ASD patient were improved by magnesium supplement (Data not shown), we measured NMDA currents related to brain magnesium as described before (Slutsky et al., 2010). ASD neurons generated significantly smaller currents in response to the focal application of NMDA. The amplitude of NMDA currents of ASD neurons at positive membrane potentials was significantly smaller (Fig. 6). In addition, NMDA receptor subunits NR1 and NR2A mRNA expression levels were significantly reduced in ASD neurons. However, the expression of NR2B was not changed (Fig. 7). NMDA receptor functions as a heterotetramer that consists of two NR1 and two NR2 subunits (Dingledine et al., 1999). Therefore, these results suggest that NMDA currents were significantly smaller in ASD neurons because the number of functional NMDA receptors was decreased by reduced NR1 expression.

CaMKIIa, NMDAR downstream signaling molecule, mRNA expression was significantly reduced in ASD neurons, but the ratio of CaMKII positive neurons and

the mean fluorescence intensity of CaMKII in neurons were not altered.

Because NMDARs are related to CaMKII activities (Bayer et al., 2001), we checked the mRNA expression level of CaMKIIa. ASD neurons expressed significantly lower CaMKIIa mRNAs (Fig. 8A). One phenotype of ASD model reported the disruption of excitatory/inhibitory balance (Gogolla et al., 2009). Therefore, we assessed whether the downregulation of CaMKIIa mRNAs leads to decreasing the number of CaMKII positive neurons. We stained neurons with CaMKII antibodies and counted the number of CaMKII positive neurons per that of GFP positive neurons. However, we observed the ratio of CaMKII positive neurons was not changed in ASD neurons (Fig. 8B). In addition, we assessed whether the downregulation of CaMKIIa mRNAs was reflected to the reduction of the mean fluorescence intensity in neurons. The mean fluorescence intensity of ASD neurons was not altered compared to that of normal neurons (Fig. 8C).

Figures

A

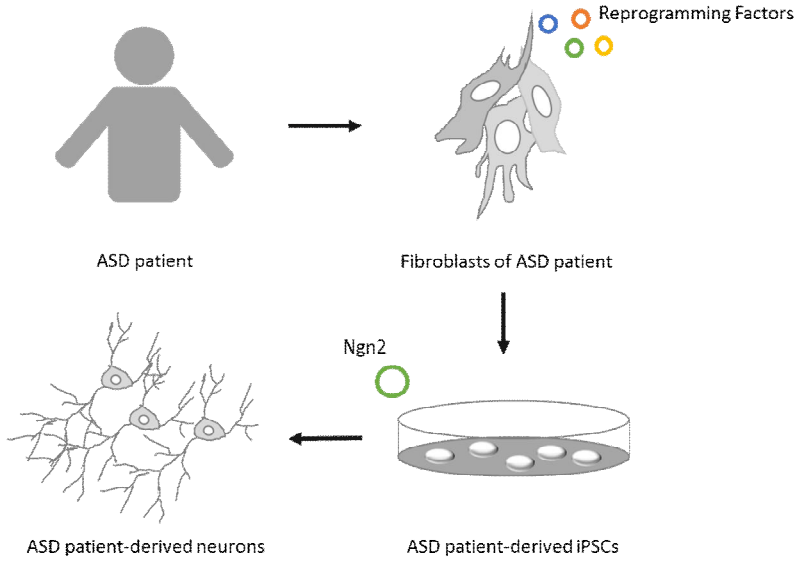

B Modified Ngn2-single step induction method

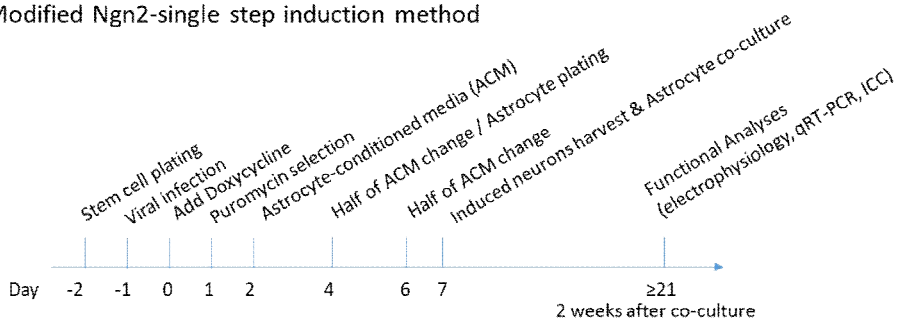

C ASD-iPSC#1 derived neurons

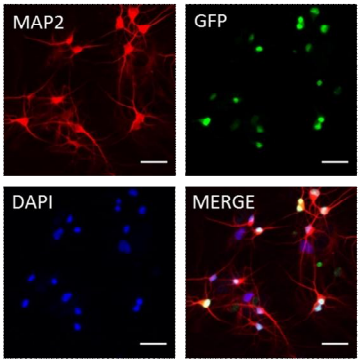

D ASD-iPSC#2 derived neurons

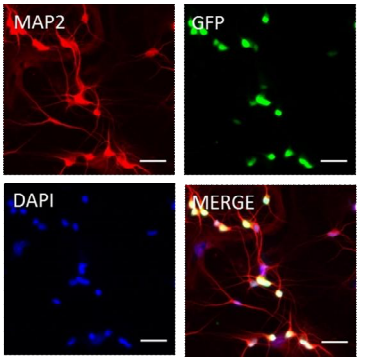

Figure 1. Experimental scheme and generation of ASD neurons

(A) Experimental scheme. Fibroblasts were obtained from the thigh of the participant diagnosed ASD by performing the skin punch biopsy. Fibroblasts of the ASD patient were reprogrammed into iPSCs using a standard reprogramming technique (Okita et al., 2011). Induced neurons were differentiated from iPSCs using a method based on rapid Neurogenin2 (Ngn2) single-step induction (Zhang et al., 2013). (B) Generation of ASD neurons. Stem cells were plated on day -2. TetO-Ngn2-P2A-EGFP-T2A-Puromycine lentivirus and rtTA lentivirus were treated to use Tet-On gene expression system on day -1. Doxycycline was added to induce gene expression on day 0. Virus-infected cells were selected by puromycin treatment on day 1. Media were replaced with astrocyte-conditioned media (ACM) on day 2. Half of the culture media was changed with ACM every 2 days until day 6. On day 4, astrocytes were prepared on other plates. Induced neurons were harvested and plated on the astrocyte culture on day 7. Half of media was changed every 2-3 days until experiments. Functional analyses including immunocytochemistry, qPCR, and electrophysiology were performed over 2 weeks after astrocyte co-culture. (C, D) Immunostaining of ASD neurons with MAP2

(neuronal marker). ASD-iPSC#1 and #2 derived neurons were stained with MAP2, GFP (to identify cells with viral transduction), and DAPI (nucleus marker). Almost 100% of GFP-positive viral-infected cells differentiated into neurons. Scale bar, 50 ㎛.

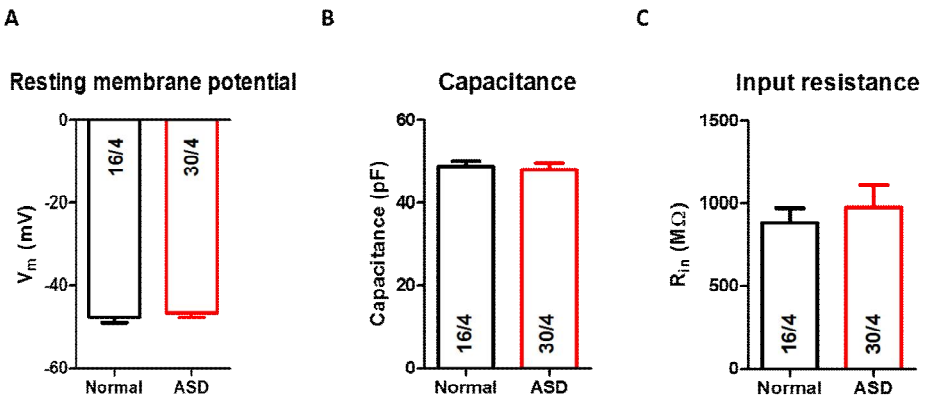
A
Resting membrane potential
0
-20
-40
-60
V_m (mV)
16/4
30/4
Normal
ASD
B
Capacitance
60
40
20
0
Capacitance (pF)
16/4
30/4
Normal
ASD
C
Input resistance
1500
1000
500
0
R_{in} (MΩ)
16/4
30/4
Normal
ASD

Figure 2. Resting membrane potential, capacitance, and input resistance were not changed in ASD neurons.

(A) Result of resting membrane potential. Resting membrane potential was not changed between normal neurons and ASD neurons (Normal: −47.69 ± 1.280 mV, n=16 cells from 2 lines; ASD: −46.67 ± 1.128 mV, n=30 cells from 2 lines). All experiments were replicated 4 times. (B) Result of capacitance. Capacitance was not changed in ASD neurons (Normal: 48.74 ± 1.225 pF, n=16; ASD: 47.95 ± 1.562 pF, n=30). (C) Result of input resistance. Input resistance of ASD neurons was not changed (Normal: 883.7 ± 92.24 MΩ, n=16; ASD: 977.4 ± 133.2 MΩ, n=30). Data were presented as mean ± SEM. Numbers of cells / independent cultures analyzed are shown in the bars.

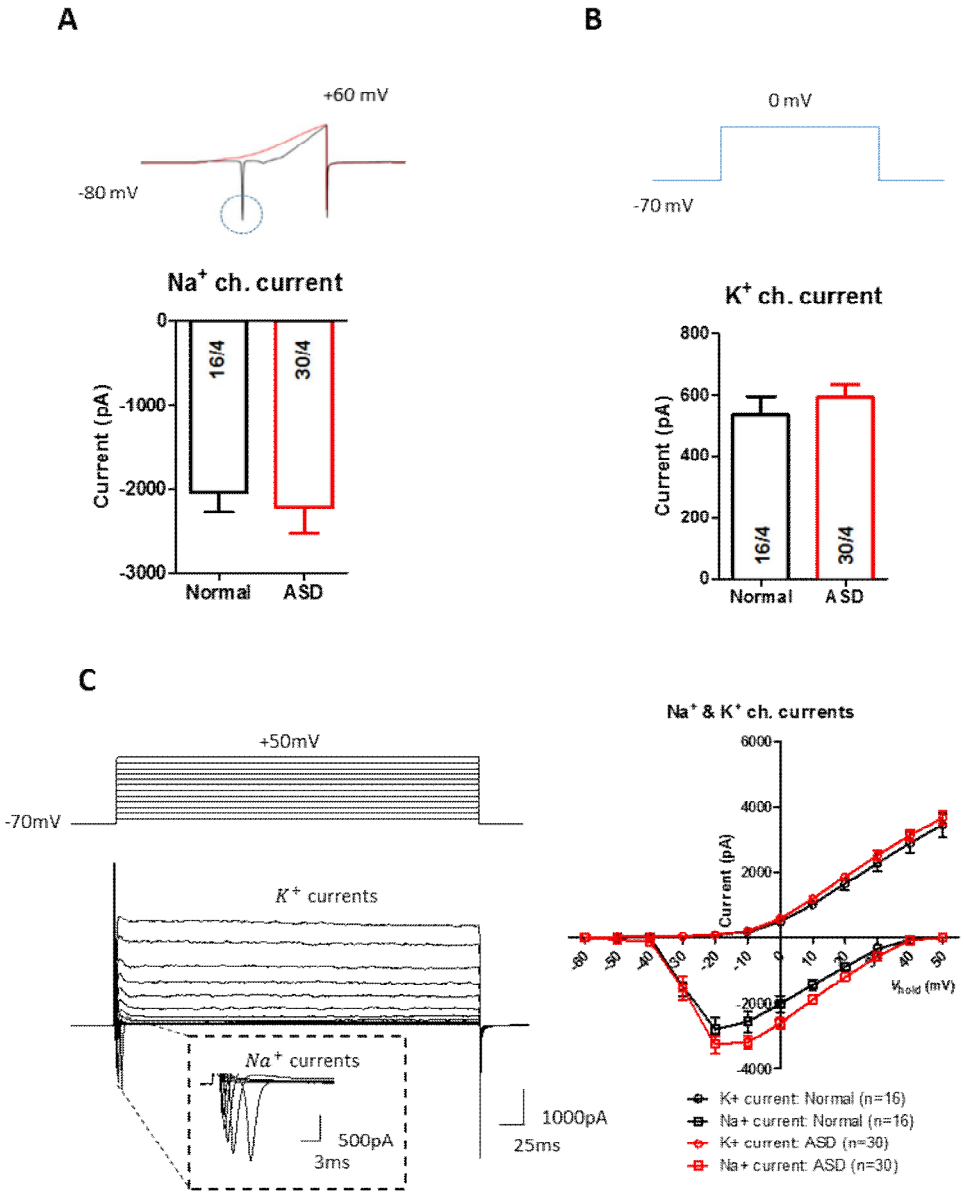
A
+60 mV
-80 mV
Na+ ch. current
Current (pA)
0
-1000
-2000
-3000
16/4
30/4
Normal
ASD
B
0 mV
-70 mV
K+ ch. current
Current (pA)
800
600
400
200
0
16/4
30/4
Normal
ASD
C
+50mV
-70mV
K+ currents
Na+ currents
500pA
3ms
1000pA
25ms
Na+ & K+ ch. currents
Current (pA)
6000
4000
2000
-2000
-4000
-60
-50
-40
-30
-20
-10
0
10
20
30
40
50
Vhold (mV)
K+ current: Normal (n=16)
Na+ current: Normal (n=16)
K+ current: ASD (n=30)
Na+ current: ASD (n=30)

Figure 3. Sodium and potassium currents were not changed in ASD neurons.

(A) Result of inward sodium currents. Sodium currents were not changed in ASD neurons compared to normal neurons (Normal: −2035 ± 232.6 pA, n=16 cells from 2 lines; ASD: −2215 ± 313.5 pA, n=30 cells from 2 lines). Upper panel is the representative trace of membrane currents recorded following a ramp depolarization protocol from −80 mV to +60 mV. (B) Result of outward potassium currents. Potassium currents were not changed in ASD neurons (Normal: 535.1 ± 61.16 pA, n=16; ASD: 594.5 ± 39.02 pA, n=30). Upper panel is the recording protocol which is step 0 mV depolarization from −70 mV holding potential. (C) Quantification of I/V curves of sodium and potassium currents in neurons (right panel). Sodium and potassium currents were not changed in ASD neurons. Neurons were recorded following 10 mV step depolarizations from −60 mV to +50 mV at −70 mV holding potential (left upper panel). Representative traces of whole−cell voltage clamp sodium and potassium currents (left lower panel). Data were presented as mean ± SEM. Numbers of cells/independent cultures analyzed are shown in the bars.

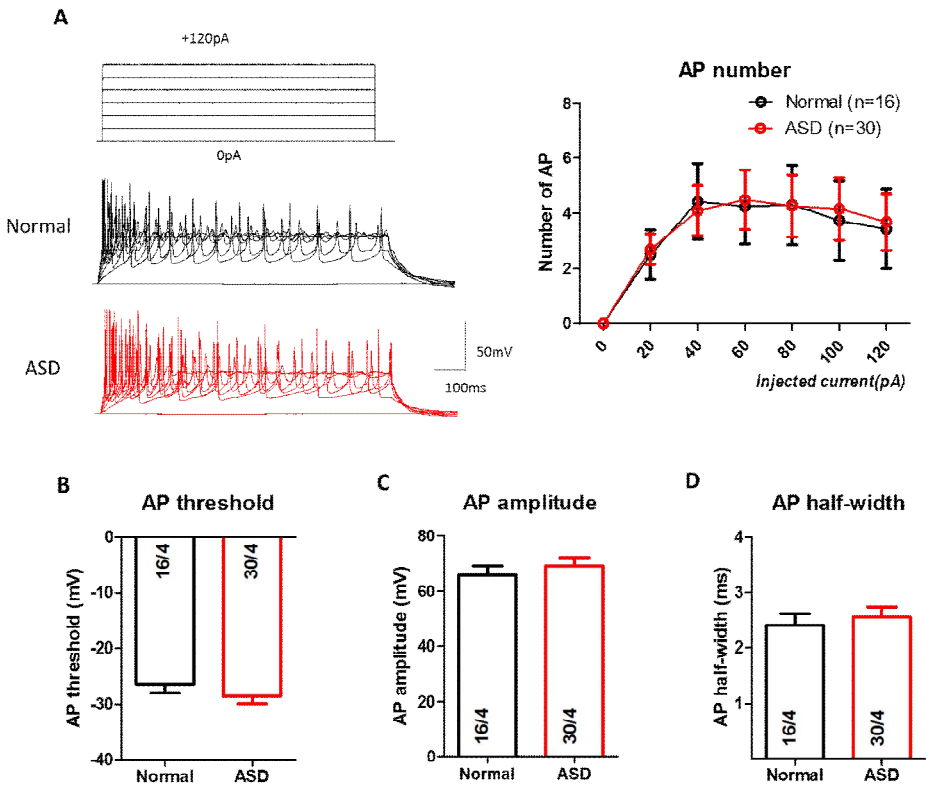
A
+120pA
0pA
Normal
ASD
50mV
100ms
AP number
Normal (n=16)
ASD (n=30)
Number of AP
Injected current(pA)
B
AP threshold
AP threshold (mV)
16/4
30/4
Normal
ASD
C
AP amplitude
AP amplitude (mV)
D
AP half-width
AP half-width (ms)

Figure 4. Neuronal excitability and action potential properties were not changed in ASD neurons.

(A) Summary plots of the AP number versus injected currents during current-clamp recordings of neurons (right panel). AP numbers were not changed in ASD neurons. Neurons were recorded following stepwise depolarizing 20 pA current injection (left upper panel). Left lower panel is each of representative traces of action potentials. (B) Result of the AP firing threshold. AP threshold was not changed in ASD neurons (Normal: −26.41 ± 1.571 mV, n=16; ASD: −28.54 ± 1.357 mV, n=30). (C) Result of the AP maximal amplitude. AP amplitude was not changed in ASD neurons (Normal: 65.80 ± 3.369 mV, n=16; ASD: 69.14 ± 3.186 mV, n=30). (D) Result of half-width of APs evoked during 800ms. AP half-width was not changed in ASD neurons (Normal: 2.409 ± 0.2114 ms, n=16; ASD: 2.560 ± 0.1811 ms, n=30). Data were presented as mean ± SEM. Numbers of cells/independent cultures analyzed are shown in the bars.

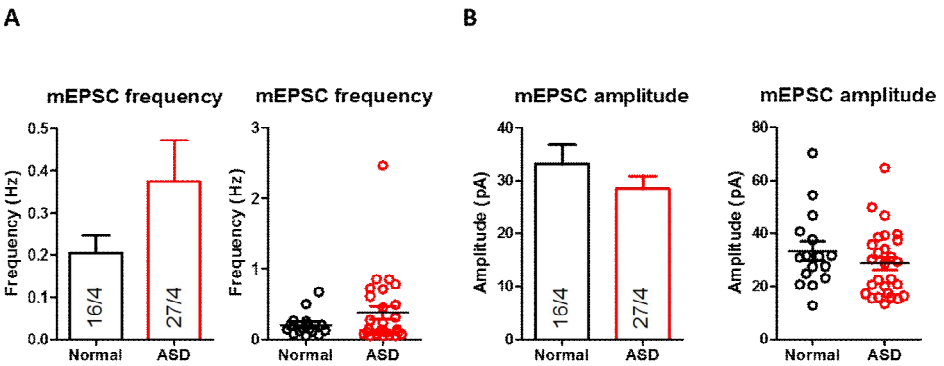
A
B
mEPSC frequency
mEPSC frequency
mEPSC amplitude
mEPSC amplitude
Frequency (Hz)
Frequency (Hz)
Amplitude (pA)
Amplitude (pA)
16/4
27/4
16/4
27/4
Normal
ASD
Normal
ASD
Normal
ASD
Normal
ASD

Figure 5. Miniature excitatory postsynaptic currents were not changed in ASD neurons.

(A) Quantification of mEPSC frequency. mEPSC frequency was not significantly changed in ASD neurons (Normal: 0.2048 ± 0.04095 Hz, n=16; ASD: 0.3758 ± 0.09626 Hz, n=27). (B) Quantification of mEPSC amplitude. mEPSC amplitude was not changed in ASD neurons (Normal: 33.12 ± 3.581 pA, n=16; ASD: 28.46 ± 2.439 pA, n=27). Data presented as the column bar graph (left panel) and the scatter plot (right panel). Data presented as mean ± SEM. Numbers of cells/independent cultures analyzed are shown in the bars.

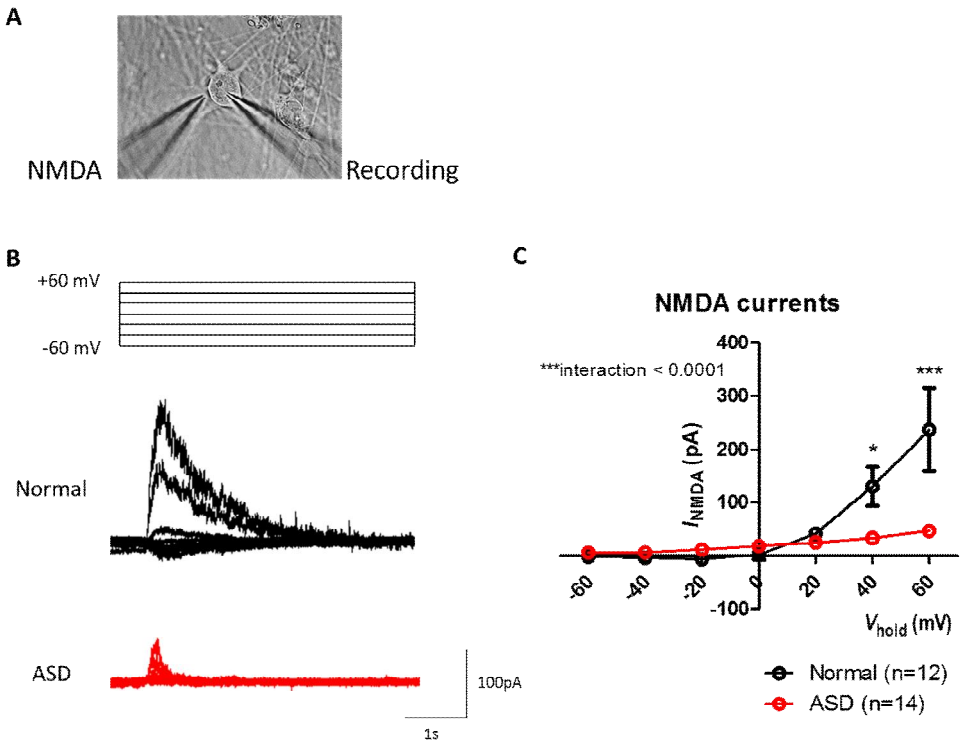
A
NMDA
Recording
B
+60 mV
-60 mV
Normal
ASD
100pA
1s
C
NMDA currents
***interaction < 0.0001
400
300
200
100
-100
I_{NMDA} (pA)
*
***
-60
-40
-20
0
20
40
60
V_{hold} (mV)
Normal (n=12)
ASD (n=14)

Figure 6. NMDA currents were significantly reduced in ASD neurons.

(A) Representative image of NMDA focal transient application during whole-cell patch recording. 100 μM NMDA and 10 μM Glycine were treated. (B) Experimental protocol and representative current traces. NMDA currents of neurons were measured at a holding potential of 20 mV stepwise change from −60 mV to +60 mV. (C) Summary plot of the peak currents versus voltage curves recorded in normal neurons and ASD neurons. NMDA currents were significantly reduced in 40 mV (Normal: 129.9 ± 36.35 pA, n=12; ASD: 32.96 ± 2.144 pA, n=14) and 60 mV (Normal: 237.0 ± 77.75 pA, n=12; ASD: 46.35 ± 4.069 pA, n=14) [$p < 0.0001$ in the holding voltage and NMDA currents interaction, two-way repeated measures ANOVA and Bonferroni post-tests, $*p < 0.05$, $***p < 0.001$]. Data were presented as mean ± SEM. Numbers of NMDA currents positive cells analyzed are shown in the symbol explanation. NMDA currents were measured in the total 3 independent cultures.

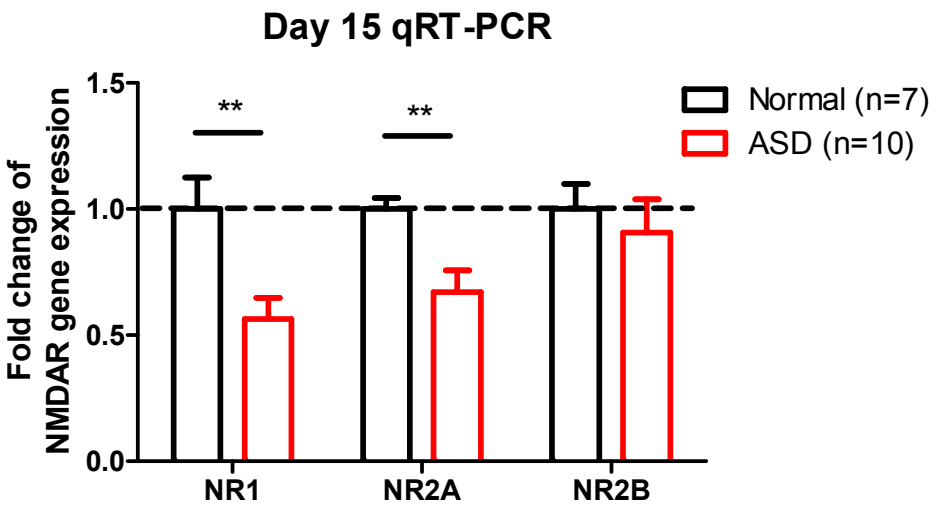
Day 15 qRT-PCR
Fold change of NMDAR gene expression
1.5
1.0
0.5
0.0
**
**
Normal (n=7)
ASD (n=10)
NR1
NR2A
NR2B

Figure 7. NMDA receptor subunits' mRNA levels expressed in ASD neurons were reduced.

Relative expression of NR1, NR2A, and NR2B mRNAs in neurons on the day 15 after co-culture. mRNAs of NR1 (Normal: 1.000 ± 0.125, n=7; ASD: 0.564 ± 0.084, n=10; unpaired *t*-test, $^{**}p < 0.01$) and NR2A (Normal: 1.000 ± 0.449, n=7; ASD: 0.669 ± 0.088, n=10; unpaired *t*-test, $^{**}p < 0.01$) were expressed significantly lower in ASD neurons. mRNA level of NR2B (Normal: 1.000 ± 0.099, n=7; ASD: 0.905 ± 0.0135, n=10) was not changed in ASD neurons. All groups were normalized by GAPDH. Data were presented as mean ± SEM. mRNAs were measured in the total 5 independent cultures.

A

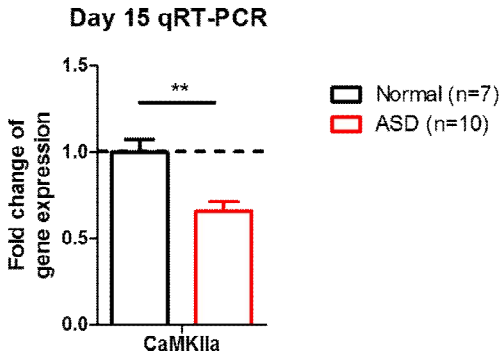
Day 15 qRT-PCR
Fold change of gene expression
1.5
1.0
0.5
0.0
**
CaMKIIa
Normal (n=7)
ASD (n=10)

B

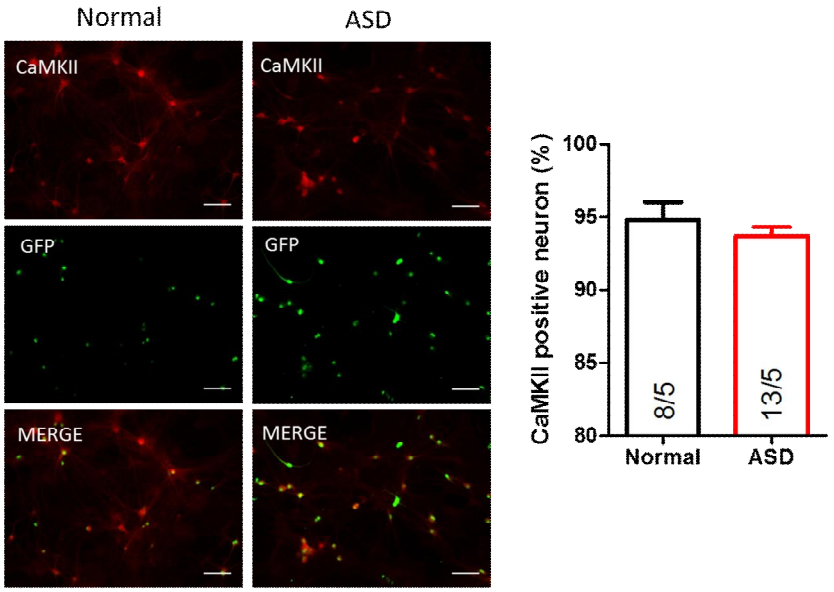
Normal
ASD
CaMKII
CaMKII
GFP
GFP
MERGE
MERGE
CaMKII positive neuron (%)
100
95
90
85
80
8/5
13/5
Normal
ASD

C

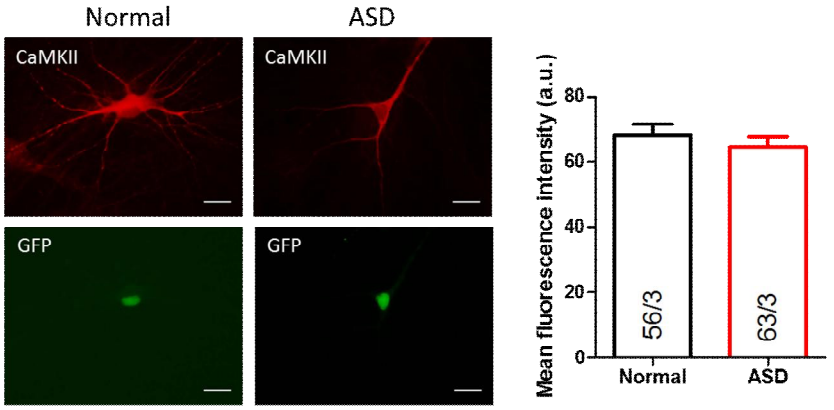
Normal
ASD
CaMKII
CaMKII
GFP
GFP
Mean fluorescence intensity (a.u.)
80
60
40
20
0
56/3
63/3
Normal
ASD

Figure 8. CaMKIIa mRNA level was reduced in ASD neurons, but the ratio of CaMKII positive neurons and the mean intensity of CaMKII in neurons were not altered.

(A) Relative expression of CaMKIIa mRNAs in neurons on the day 15 after co-culture. The mRNA level of CaMKII (Normal: 1.000 ± 0.075, n=7; ASD: 0.658 ± 0.056, n=10; unpaired *t*-test, $**p < 0.01$) was reduced in ASD neurons. All groups were normalized by GAPDH. The mRNAs were measured in the total 5 independent cultures. (B) The ratio of CaMKII positive neurons. Neurons were stained with CaMKIIa antibodies. The ratio of CaMKII-positive per GFP-positive neurons (Normal: 94.82 ± 1.186 %, n=8; ASD: 93.74 ± 0.593 %, n=13) was not changed in ASD neurons. GFP identifies cells with viral transduction. Numbers of coverslips/independent cultures analyzed are shown in the bars. Scale bar, 25 ㎛. (C) The mean fluorescence intensity of CaMKII in neurons. The mean fluorescence intensity of stained CaMKII (Normal: 68.17 ± 3.227, n=56; ASD: 64.51 ± 3.278, n=63) was not changed in ASD neurons. Data were presented as mean ± SEM. Numbers of cells/independent cultures analyzed are shown in the bars. Scale bar, 100 ㎛.

Discussion

We investigated cellular phenotypes of human ASD neurons. Intrinsic nine electrical parameters including resting membrane potential, capacitance, input resistance, sodium/potassium currents, AP numbers, AP threshold, AP amplitude, and AP half-width which reflect neuronal maturation were not changed in ASD neurons at 2 weeks after co-culture (Fig. 2, 3, 4). We could conclude that the neuronal maturation reaches the similar state over 2 weeks after co-culture. However, ASD patients and ASD models commonly show immaturity of neuronal precursors and pyramidal neurons (Wegiel et al., 2010). If intrinsic electrical parameters were measured at the early stages such as 2-3 days after co-culture and one week after co-culture as described before (Chanda et al., 2014; Pang et al., 2011), we might be able to quantify the degree of maturation.

The amplitude and frequency of miniature excitatory postsynaptic currents(mEPSCs) did not show significant differences between ASD and normal neurons (Fig. 5). However, NMDA currents from ASD neurons were significantly reduced in response to the focal application (Fig. 6). In the previous study related to Phelan-McDermid syndrome(PMDS), PMDS neurons showed reduced the amplitude and frequency of spontaneous EPSC. Also, both AMPA-

EPSCs and NMDA-EPSCs were impaired in PMDS neurons (Shcheglovitov et al., 2013). To confirm details underlying excitatory synaptic transmission, we should measure AMPA currents from ASD neurons. It is possible that AMPA currents are enhanced in ASD neurons unlikely NMDA currents. Another possibility is that synaptic NMDARs are not altered, but extrasynaptic NMDARs are reduced in ASD neurons. Synaptic and extrasynaptic NMDARs were known as performing opposing roles in neuronal calcium signaling and BDNF gene regulation (Vanhoutte and Bading, 2003). Activation of synaptic NMDA receptors causes CREB activation, induction of BDNF gene expression, pro-survival programs, and synaptic plasticity. Oppositely, activation of extrasynaptic NMDA receptors induces CREB shut-off, inhibition of BDNF gene expression, and cell death pathways (Hardingham et al., 2002). Therefore, to confirm the functions of which NMDA receptors were weaken in ASD neurons, we need to check the phosphorylation level of CREB and the protein level of BDNF.

Infantile mineral imbalances including magnesium were suggested as one of the causes of ASD (Yasuda and Tsutsui, 2013). In the case of the ASD patient participated in this study, magnesium supplement improved symptoms including self-injury and repetitive behaviors (Data not shown). If we measure mineral changes before and after magnesium supplement in the patient, it might be helpful to check the possibility of mineral imbalances.

The main phenotype of ASD neurons is related to NMDA receptor

signaling. NMDA currents were significantly reduced in ASD neurons (Fig. 6). The mRNA expression levels of NMDA receptor subunits, NR1 and NR2A were decreased, but that of NR2B was not changed (Fig. 7). In addition, the mRNA level of CaMKII was also reduced (Fig. 8A). In the previous study, NR2B-containing NMDARs bind to CaMKII with high affinity, so they enhance long-term potentiation (LTP). However, NR2A-containng NMDARs that bind to CaMKII with low affinity show dramatically reducing LTP (Barria and Malinow, 2005). Some researchers suggest the faster kinetics of NR2A-containing NMDARs allow less calcium entry (Quinlan et al., 2004). Furthermore, elevating magnesium increased NMDA currents, upregulated NR2B, and enhanced NMDAR-dependent signaling (Slutsky et al., 2010). One possibility is that ASD neurons could be partially rescued by treating magnesium. Supplemented magnesium could increase NR2B-containing NMDAR. Increased NR2B-containing NMDARs allow more calcium entry. More calcium entry by NR2B-containing NMDARs induces activation of CaMKII.

A lot of ASD mouse models showed circuit defects of excitatory and inhibitory balance (Gogolla et al., 2009). Therefore, we tested that reduced CaMKII mRNA level decreases the number of excitatory neurons in ASD. We observed that the number of CaMKII-positive excitatory neurons was not changed (Fig. 8B). In addition, we measured the mean fluorescence intensity of CaMKII in the cell bodies to confirm whether intracellular CaMKII was

decreased in ASD neurons. However, we did not observe any changes in the mean fluorescence intensity of CaMKII (Fig. 8C). One possibility is that CaMKII mRNA level was decreased, but the protein level was not altered. Because CaMKII activity is regulated by phosphorylation and dephosphorylation, CaMKII mRNA level might not directly reflect to CaMKII protein level. Another possibility is that the mean fluorescence intensity of CaMKII in the cell bodies is not affected because the synaptic translocation of CaMKII is impaired in ASD neurons. To confirm these possibilities, we need to compare CaMKII protein level of synaptosomal fraction between normal and ASD neurons.

In summary, although quantification of various proteins remains, we observed reduced NMDA currents in ASD neurons. Our finding suggests a possibility that ASD neurons are disrupted in NMDAR related signaling.

References

Abrahams, B.S., and Geschwind, D.H. (2008). Advances in autism genetics: on the threshold of a new neurobiology. Nature reviews Genetics *9*, 341–355.

Barria, A., and Malinow, R. (2005). NMDA receptor subunit composition controls synaptic plasticity by regulating binding to CaMKII. Neuron *48*, 289–301.

Bayer, K.U., De Koninck, P., Leonard, A.S., Hell, J.W., and Schulman, H. (2001). Interaction with the NMDA receptor locks CaMKII in an active conformation. Nature *411*, 801–805.

Bey, A.L., and Jiang, Y.H. (2014). Overview of mouse models of autism spectrum disorders. Current protocols in pharmacology *66*, 5 66 61–26.

Chanda, S., Ang, C.E., Davila, J., Pak, C., Mall, M., Lee, Q.Y., Ahlenius, H., Jung, S.W., Sudhof, T.C., and Wernig, M. (2014). Generation of induced neuronal cells by the single reprogramming factor ASCL1. Stem cell reports *3*, 282–296.

Christensen, D.L., Baio, J., Van Naarden Braun, K., Bilder, D., Charles, J., Constantino, J.N., Daniels, J., Durkin, M.S., Fitzgerald, R.T., Kurzius-Spencer, M., *et al.* (2016). Prevalence and Characteristics of Autism Spectrum Disorder Among Children Aged 8 Years--Autism and Developmental Disabilities Monitoring Network, 11 Sites, United States, 2012. Morbidity and mortality

weekly report Surveillance summaries *65*, 1-23.

Croen, L.A., Grether, J.K., Yoshida, C.K., Odouli, R., and Hendrick, V. (2011). Antidepressant use during pregnancy and childhood autism spectrum disorders. Archives of general psychiatry *68*, 1104-1112.

Dingledine, R., Borges, K., Bowie, D., and Traynelis, S.F. (1999). The glutamate receptor ion channels. Pharmacological reviews *51*, 7-61.

Fakhoury, M. (2015). Autistic spectrum disorders: A review of clinical features, theories and diagnosis. International journal of developmental neuroscience : the official journal of the International Society for Developmental Neuroscience *43*, 70-77.

Gaspard, N., Bouschet, T., Herpoel, A., Naeije, G., van den Ameele, J., and Vanderhaeghen, P. (2009). Generation of cortical neurons from mouse embryonic stem cells. Nature protocols *4*, 1454-1463.

Gogolla, N., Leblanc, J.J., Quast, K.B., Sudhof, T.C., Fagiolini, M., and Hensch, T.K. (2009). Common circuit defect of excitatory-inhibitory balance in mouse models of autism. Journal of neurodevelopmental disorders *1*, 172-181.

Hardingham, G.E., Fukunaga, Y., and Bading, H. (2002). Extrasynaptic NMDARs oppose synaptic NMDARs by triggering CREB shut-off and cell death pathways. Nature neuroscience *5*, 405-414.

Hodgkin, A.L., and Katz, B. (1949). The effect of sodium ions on the electrical activity of giant axon of the squid. The Journal of physiology *108*, 37-77.

Kim, Y.S., Leventhal, B.L., Koh, Y.J., Fombonne, E., Laska, E., Lim, E.C., Cheon, K.A., Kim, S.J., Kim, Y.K., Lee, H., *et al.* (2011). Prevalence of autism spectrum disorders in a total population sample. The American journal of psychiatry *168*, 904–912.

Klauck, S.M. (2006). Genetics of autism spectrum disorder. European journal of human genetics : EJHG *14*, 714–720.

Lamas, J.A., Reboreda, A., and Codesido, V. (2002). Ionic basis of the resting membrane potential in cultured rat sympathetic neurons. Neuroreport *13*, 585–591.

Lyall, K., Schmidt, R.J., and Hertz-Picciotto, I. (2014). Maternal lifestyle and environmental risk factors for autism spectrum disorders. International journal of epidemiology *43*, 443–464.

Maroof, A.M., Keros, S., Tyson, J.A., Ying, S.W., Ganat, Y.M., Merkle, F.T., Liu, B., Goulburn, A., Stanley, E.G., Elefanty, A.G., *et al.* (2013). Directed differentiation and functional maturation of cortical interneurons from human embryonic stem cells. Cell stem cell *12*, 559–572.

Mertens, J., Wang, Q.W., Kim, Y., Yu, D.X., Pham, S., Yang, B., Zheng, Y., Diffenderfer, K.E., Zhang, J., Soltani, S., *et al.* (2015). Differential responses to lithium in hyperexcitable neurons from patients with bipolar disorder. Nature *527*, 95–99.

Okita, K., Matsumura, Y., Sato, Y., Okada, A., Morizane, A., Okamoto, S., Hong, H., Nakagawa, M., Tanabe, K., Tezuka, K., *et al.* (2011). A more efficient method to generate integration-free human iPS cells. Nature methods *8*, 409–412.

Pang, Z.P., Yang, N., Vierbuchen, T., Ostermeier, A., Fuentes, D.R., Yang, T.Q., Citri, A., Sebastiano, V., Marro, S., Sudhof, T.C., *et al.* (2011). Induction of human neuronal cells by defined transcription factors. Nature *476*, 220–223.

Pre, D., Nestor, M.W., Sproul, A.A., Jacob, S., Koppensteiner, P., Chinchalongporn, V., Zimmer, M., Yamamoto, A., Noggle, S.A., and Arancio, O. (2014). A time course analysis of the electrophysiological properties of neurons differentiated from human induced pluripotent stem cells (iPSCs). PloS one *9*, e103418.

Quinlan, E.M., Lebel, D., Brosh, I., and Barkai, E. (2004). A molecular mechanism for stabilization of learning-induced synaptic modifications. Neuron *41*, 185–192.

Shcheglovitov, A., Shcheglovitova, O., Yazawa, M., Portmann, T., Shu, R., Sebastiano, V., Krawisz, A., Froehlich, W., Bernstein, J.A., Hallmayer, J.F., *et al.* (2013). SHANK3 and IGF1 restore synaptic deficits in neurons from 22q13 deletion syndrome patients. Nature *503*, 267–271.

Slutsky, I., Abumaria, N., Wu, L.J., Huang, C., Zhang, L., Li, B., Zhao, X., Govindarajan, A., Zhao, M.G., Zhuo, M., *et al.* (2010). Enhancement of learning and memory by elevating brain magnesium. Neuron *65*, 165–177.

Takahashi, K., Tanabe, K., Ohnuki, M., Narita, M., Ichisaka, T., Tomoda, K., and Yamanaka, S. (2007). Induction of pluripotent stem cells from adult human fibroblasts by defined factors. Cell *131*, 861–872.

Takahashi, K., and Yamanaka, S. (2006). Induction of pluripotent stem cells from mouse embryonic and adult fibroblast cultures by defined factors. Cell *126*, 663–676.

Telias, M., Segal, M., and Ben-Yosef, D. (2014). Electrical maturation of neurons derived from human embryonic stem cells. F1000Research *3*, 196.

Vanhoutte, P., and Bading, H. (2003). Opposing roles of synaptic and extrasynaptic NMDA receptors in neuronal calcium signalling and BDNF gene regulation. Current opinion in neurobiology *13*, 366–371.

Wegiel, J., Kuchna, I., Nowicki, K., Imaki, H., Wegiel, J., Marchi, E., Ma, S.Y., Chauhan, A., Chauhan, V., Bobrowicz, T.W., *et al.* (2010). The neuropathology of autism: defects of neurogenesis and neuronal migration, and dysplastic changes. Acta neuropathologica *119*, 755–770.

Wen, Z., Nguyen, H.N., Guo, Z., Lalli, M.A., Wang, X., Su, Y., Kim, N.S., Yoon, K.J., Shin, J., Zhang, C., *et al.* (2014). Synaptic dysregulation in a human iPS cell model of mental disorders. Nature *515*, 414–418.

Yasuda, H., and Tsutsui, T. (2013). Assessment of infantile mineral imbalances in autism spectrum disorders (ASDs). International journal of environmental research and public health *10*, 6027–6043.

Yu, J., Vodyanik, M.A., Smuga-Otto, K., Antosiewicz-Bourget, J., Frane, J.L., Tian, S., Nie, J., Jonsdottir, G.A., Ruotti, V., Stewart, R., *et al.* (2007). Induced pluripotent stem cell lines derived from

human somatic cells. Science *318*, 1917–1920.

Yu, N.K., Kim, H.F., Shim, J., Kim, S., Kim, D.W., Kwak, C., Sim, S.E., Choi, J.H., Ahn, S., Yoo, J., *et al.* (2016). A transducible nuclear/nucleolar protein, mLLP, regulates neuronal morphogenesis and synaptic transmission. Scientific reports *6*, 22892.

Zhang, Y., Pak, C., Han, Y., Ahlenius, H., Zhang, Z., Chanda, S., Marro, S., Patzke, C., Acuna, C., Covy, J., *et al.* (2013). Rapid single–step induction of functional neurons from human pluripotent stem cells. Neuron *78*, 785–798.

Zhu, L., Wang, X., Li, X.L., Towers, A., Cao, X., Wang, P., Bowman, R., Yang, H., Goldstein, J., Li, Y.J., *et al.* (2014). Epigenetic dysregulation of SHANK3 in brain tissues from individuals with autism spectrum disorders. Human molecular genetics *23*, 1563–1578.

초 록

자폐 스펙트럼 장애(ASD, Autism Spectrum Disorder)는 사회적인 의사소통과 상호작용의 결함, 제한적이고 반복적인 행동 패턴을 보이고, 전 세계적으로 유병률이 1%에 이르는 발달장애이다. 지금까지 자폐 스펙트럼 장애에 대한 대부분의 연구는 질환 마우스 모델을 기반으로 하였다. 그러나 자폐 스펙트럼 장애의 원인은 복합적이고 마우스 모델의 부적합성 때문에 마우스 모델에서 약효를 확인한 물질이 임상단계에서 실패하는 경우가 많았다. 최근 유도만능 줄기세포(iPSCs, induced Pluripotent Stem Cells)분야에서 기술적인 발전은 사람 모델에서 연구를 가능하게 하였다.

이 연구에서 우리는 자폐 스펙트럼 장애 환자에서 유래한 유도만능줄기세포로부터 사람 신경세포를 만들었고, 건강한 사람으로부터 만든 뉴런과 비교하여 어떠한 세포학적 차이가 있는지 확인하였다. 특히 주목할 만한 점은 자폐 스펙트럼 장애 환자 유래 신경세포에서 기억과 학습에 연관된다고 알려진 NMDA 전위가 감소하였고, NMDA수용체의 발현 양이 감소한 것을 확인하였다. 또한, NMDA수용체 신호전달 하위 물질인 CaMKII의 발현 양도 감소한 것을 확인하였다. 종합하면, 자폐 스펙트럼 장애 환자에서 유래한 신경세포에서 NMDA수용체 신호전달과 관련된 결함을 확인하였다.

주요어: 자폐 스펙트럼 장애(ASD), 유도만능줄기세포(iPSCs), 사람 신경세포, NMDA 전위, CaMKII

학 번: 2014-21279